

# Denoising Vision Transformer Autoencoder with Spectral Self-Regularization

Xunzhi Xiang<sup>1\*†</sup>, Xingye Tian<sup>2†</sup>, Guiyu Zhang<sup>3</sup>, Yabo Chen<sup>4</sup>, Shaofeng Zhang<sup>5</sup>  
 Xuebo Wang<sup>2</sup>, Xin Tao<sup>2</sup>, Qi Fan<sup>1‡</sup>

<sup>1</sup>Nanjing University, <sup>2</sup>Kling Team, Kuaishou Technology

<sup>3</sup>Chinese University of Hong Kong, Shenzhen, <sup>4</sup>Shanghai Jiao Tong University

<sup>5</sup>University of Science and Technology of China

## Abstract

*Variational autoencoders (VAEs) typically encode images into a compact latent space, reducing computational cost but introducing an optimization dilemma: a higher-dimensional latent space improves reconstruction fidelity but often hampers generative performance. Recent methods attempt to address this dilemma by regularizing high-dimensional latent spaces using external vision foundation models (VFs). However, it remains unclear how high-dimensional VAE latents affect the optimization of generative models. To our knowledge, our analysis is the first to reveal that redundant high-frequency components in high-dimensional latent spaces hinder the training convergence of diffusion models and, consequently, degrade generation quality. To alleviate this problem, we propose a spectral self-regularization strategy to suppress redundant high-frequency noise while simultaneously preserving reconstruction quality. The resulting Denoising-VAE, a ViT-based autoencoder that does not rely on VFs, produces cleaner, lower-noise latents, leading to improved generative quality and faster optimization convergence. We further introduce a spectral alignment strategy to facilitate the optimization of Denoising-VAE-based generative models. Our complete method enables diffusion models to converge approximately 2× faster than with SD-VAE, while achieving state-of-the-art reconstruction quality ( $rFID = 0.28$ ,  $PSNR = 27.26$ ) and competitive generation performance ( $gFID = 1.82$ ) on the ImageNet 256×256 benchmark.*

## 1. Introduction

Latent diffusion models [3, 36, 38, 52] have demonstrated strong performance in high-quality image and video synthesis. These models typically operate in compressed latent

\*This work was conducted during the author's internship at Kling Team, Kuaishou Technology

†Equal Contribution

‡Corresponding author

spaces to reduce computational costs associated with high-resolution image generation.

Diffusion models generally comprise two sequential modules. First, a variational autoencoder (VAE) [24], also referred to as a visual tokenizer [2, 16], encodes the input image into a compact, low-resolution latent representation. Then, a generative model [5, 31, 35] is trained on the encoded latent space [11, 29], reducing computational overhead and enabling high-quality image generation. However, VAEs face a trade-off dilemma [10, 15, 22, 53]: higher-dimensional latent representations improve reconstruction quality for diffusion models, but the resulting high computational complexity usually impedes optimization and consequently degrades generative performance.

Some works [7, 53] attempt to mitigate this problem by employing VFs [4, 16, 33, 37, 59] to regularize high-dimensional latent spaces. Despite empirical success, the root cause of this trade-off remains unclear, limiting a deeper understanding of diffusion models.

To investigate this issue, we conduct a preliminary analysis. We use a VAE to encode a uniform-color image and visualize its latent representation using principal component analysis (PCA). As shown in Figure 1, the encoded latent representation exhibits noticeable artifacts. As latent dimensionality increases, the artifacts become more pronounced, suggesting that the encoder introduces input-independent high-frequency noise—an effect further amplified in higher-dimensional latent spaces.

We hypothesize that high-frequency noise increases optimization complexity, thereby hindering the convergence of diffusion models. To address this, we propose actively denoising and smoothing the latent space while preserving reconstruction quality, yielding well-structured high-dimensional VAE latents for high-quality image generation. Specifically, we introduce Denoising-VAE, a ViT-based [13, 46], VFM-free autoencoder that regularizes the high-dimensional latent space through Spectral Self-Regularization.

In Denoising-VAE, spectral regularization is applied to

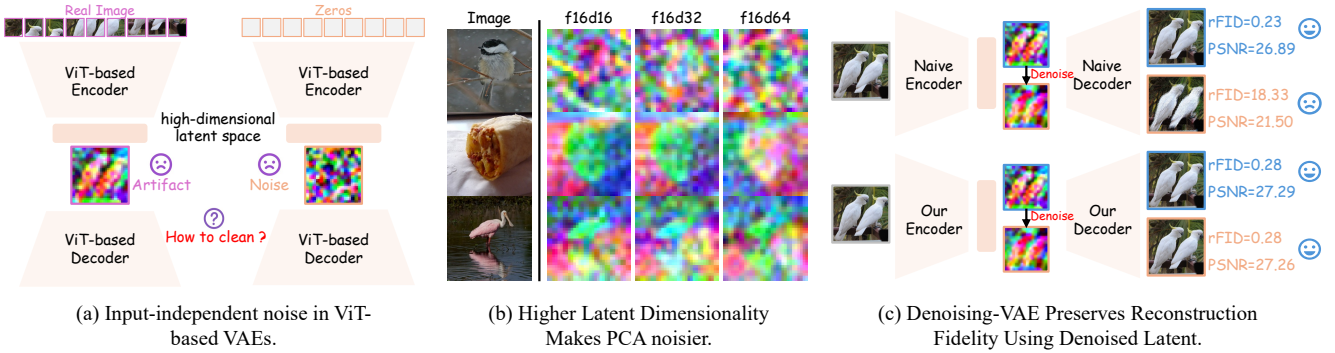


Figure 1. Frequency-domain analysis of ViT-based VAE latent spaces and comparison with convolutional baselines. (a) Encoding a uniform-color image with a ViT-based tokenizer yields structured high-frequency artifacts in the latent space, revealing input-independent noise injected during tokenization. (b) As latent dimensionality increases, PCA projections of ViT-based latents become increasingly noisy and spatially unstable, indicating the amplification of undesired high-frequency variation. (c) In contrast, Conventional VAEs show strong dependence on high-frequency latent signals, where reconstruction fidelity is tightly coupled to noise patterns.

the latent space during autoencoder training. Spectral regularization encourages the model to reconstruct high-quality images from both original and low-pass filtered latent representations. This constraint suppresses redundant high-frequency noise while maintaining reconstruction quality in VAEs. It enables VAEs to produce cleaner, lower-noise high-dimensional latents, leading to improved generative performance and faster optimization convergence. In addition, we propose Frequency-Aware Diffusion Alignment (FDA) to accelerate the optimization of Denoising-VAE-based diffusion models. During generative model training, FDA generates low-pass filtered latent representations at multiple frequency bands and aligns noisy latents with their corresponding clean counterparts.

Unlike prior VAE approaches [7, 53], we identify high-frequency noise as the root cause of the optimization dilemma in high-dimensional latent spaces and mitigate it through lightweight spectral self-regularization. On the ImageNet 256×256 benchmark, Denoising-VAE achieves state-of-the-art reconstruction performance (rFID: 0.28, PSNR: 27.26), outperforming the best ViT-based alternative [56] by 2.88 dB in PSNR, while maintaining competitive generative performance (gFID: 1.82). Additionally, our high-dimensional VAE (32 channels) enables diffusion models to converge nearly 2× faster than the conventional convolutional SD-VAE [38] (4 channels), while reducing total autoencoder GFLOPs by 5.75×. These results demonstrate the efficiency and scalability advantages of our spectral regularization method.

Overall, our work delivers the following contributions:

- We empirically show that ViT-based VAEs exhibit persistent high-frequency noise in the latent space, which intensifies with increasing latent dimensionality.
- We introduce Spectral Regularization to denoise the latent space, yielding cleaner, structurally constrained latents and easing diffusion optimization.

- We propose Frequency-Domain Diffusion Alignment accelerating diffusion convergence.

## 2. Related Work

**Latent Generative Models.** Latent generative models have established a foundation for high-fidelity image synthesis. Continuous VAEs [24, 25, 27] learn smooth latent spaces with Gaussian priors, while VQ-VAE models [8, 45] discrete representations using a vector-quantized codebook coupled with an autoregressive decoder. Following the discrete paradigm, VQGAN [14] enhances reconstruction through adversarial training and transformer-based autoregressive modeling. MaskGIT [5] further accelerates the generation of discrete latents by introducing a masked token prediction schedule that enables parallel decoding. Alternatively, Latent Diffusion Models (LDM) [36, 38] apply diffusion processes directly in a compressed latent space, enabling efficient and scalable high-resolution synthesis. Among these, the Diffusion Transformer (DiT) [35] demonstrates the strong suitability of transformer architectures for diffusion-based generation. Building on DiT, the SiT [31] model incorporates flexible interpolation mechanisms for versatile distribution mapping and improved modularity.

**Image Tokenizer.** Image tokenizers map images into latents that are simpler to handle than pixels in generative modeling. Early image tokenizers can be grouped into continuous and discrete two classes. Continuous tokenizers, typically variational autoencoders, learn Gaussian-prior latent spaces at reduced spatial resolution and are widely used for latent diffusion. In contrast, discrete tokenizers [49, 50] such as VQ-VAE [45] instantiate vector-quantized codebooks and emit index sequences for autoregressive decoders. Recent work targets higher compression ratios and improved reconstruction fidelity while preserving downstream generative performance. DC-AE [9] and DC-AE-1.5 [10] increase the spatial compression ratio to improve dif-

fusion efficiency. VAVAE [53] enlarges the latent channel dimensionality and uses vision-foundation-model regularization to enhance reconstruction, while EQ-VAE [26] applies scale equivariance regularization to improve compatibility with diffusion training. In contrast, we analyze the reconstruction-generation trade-off from a frequency viewpoint and find that the degradation at higher dimensionality is driven by excess high-frequency energy. We therefore introduce Spectral Regularization to denoise the latent space, suppressing irrelevant high-frequency components and improving diffusion optimization without external VFM.

**Latent Equivariance.** A closely related line of work [26, 42] enforces *spatial equivariance* in the latent space to obtain generator-friendly representations through predictable geometric transformations. In contrast, our objective is to directly denoise the latent representation by suppressing redundant high-frequency noise while ensuring that the denoised latent can still reconstruct a perceptually equivalent image. This frequency-domain formulation focuses on improving latent quality and stability, providing cleaner representations that better support generative modeling without compromising reconstruction fidelity.

### 3. Denoising-VAE

#### 3.1. Multi-Level Spectral Regularization

This section aims to directly simplify the high-dimensional latent space by applying low-pass filtering to suppress high-frequency noise and obtain cleaner representations. The denoised latents are then used for image reconstruction. However, in conventional VAE training, requiring both the original and denoised latents to reconstruct the exact same input image often leads to unstable optimization. Motivated by human visual perception, we relax this constraint. Human vision is more sensitive to low-frequency distortions, such as errors in object contours or shading, than to high-frequency details like fine textures. Therefore, we only require the denoised latents to reconstruct images that are perceptually equivalent to the original, rather than exactly matching it pixel by pixel.

To realize this perceptual reconstruction strategy, we propose *Multi-Level Spectral Regularization (MLSR)*. MLSR operates in the frequency domain to progressively suppress redundant high-frequency noise in the latent space while preserving perceptually important low-frequency information. At each level, it aligns denoised latents with their corresponding low-frequency reconstructions, encouraging spectral consistency and stabilizing optimization. This process suppresses redundant high-frequency noise that hinders convergence, resulting in cleaner latents and improved generative performance.

**Multi-level Spectral Regularization.** For each training image  $x$ , we define a pair of *matched* operators indexed by

an attenuation level  $\ell \in \{0, 1, 2, 3\}$ : a latent-space operator  $\mathcal{S}_\ell$  that suppresses high-frequency energy, and an image-space operator  $\mathcal{G}_\ell$  that applies a perceptually calibrated low-pass of the equivalent strength. Specifically, let  $z = \mathcal{E}(x)$  denote the latent representation of the input  $x$ , and let  $\mathcal{D}(z)$  denote the reconstruction of input image. At each training step, we *uniformly* sample one level,

$$\ell \sim \text{Unif}\{0, 1, 2, 3\}, \quad (1)$$

and ensure the decoded image from the attenuated latent matches the spectrally simplified original:

$$\mathcal{L}_{\text{spec}} = d((\mathcal{D}(\mathcal{S}_\ell(z))), \mathcal{G}_\ell(x)), \quad (2)$$

where  $d(\cdot, \cdot)$  is a weighted combination of pixel-wise MSE loss, perceptual loss [20, 30, 41], adversarial (GAN) loss [14], and a latent-space KL loss.

**Latent operator.** We suppress high-frequency components in the latent space while preserving low frequencies. Given a latent representation  $z$ , we: (i) apply a 2D Fourier transform  $\mathcal{F}$ , (ii) attenuate only the highest-magnitude frequency components according to the attenuation level, and (iii) apply the inverse transform  $\mathcal{F}^{-1}$  to map back to the spatial domain. This is implemented as:

$$\mathcal{S}_\ell(z) = \mathcal{F}^{-1}(\mathcal{M}_\ell \odot \mathcal{F}(z)), \quad (3)$$

where  $\odot$  denotes element-wise multiplication, and  $\mathcal{M}_\ell$  is a frequency-domain mask that preserves all low-frequency components. In practice, we choose  $\ell$  uniformly from  $\{0, 1, 2, 3\}$ , corresponding to 0%, 25%, 50%, and 75% high-frequency attenuation. This operation reduces latent noise while retaining perceptually important structure.

**Image operator.** To ensure perceptual consistency between latent-space suppression and the image domain, we create a corresponding reference image using adaptive Gaussian blurring. This is implemented as:

$$\mathcal{G}_\ell(x) = \text{GaussianBlur}(x; \sigma_\ell). \quad (4)$$

Implementation-wise, we blur each channel using a separable Gaussian with reflection padding to avoid edge artifacts. We choose  $\ell$  uniformly from  $\{0, 1, 2, 3\}$ , corresponding to blur levels  $\sigma_\ell = 0, 0.05, 0.25, 0.5$ . This ensures the image target aligns with the degree of latent denoising and discourages the decoder from overfitting to imperceptible details.

#### 3.2. Denoising Latents for Generation

Latent representations in high-dimensional VAEs contain large amounts of redundant high-frequency noise. This noise does not contribute to image semantics but significantly complicates the learning dynamics of diffusion models, which must implicitly fit both meaningful structure and input-independent artifacts. Approaches grounded in equivariance focus primarily on geometric consistency and do

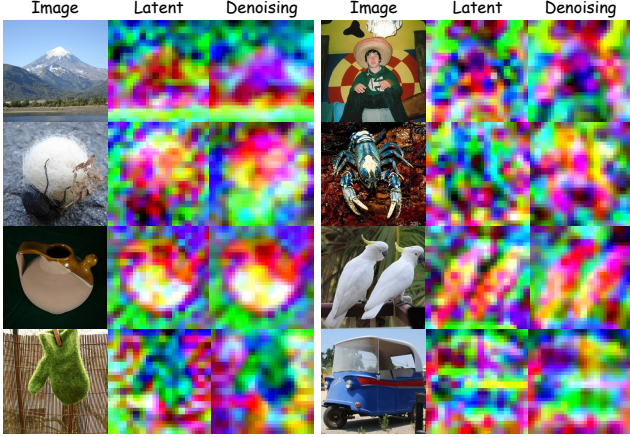


Figure 2. Per-image latent denoising with Denoising-VAE. After Spectral Regularization reveal smoother, more coherent structure.

not address the fundamental issue of noisy latent distributions, since the original latents remain the supervision target throughout training. Our approach takes a different perspective: instead of regularizing latent geometry, we directly clean the latent space. Multi-Level Spectral Regularization (Sec. 3.1) removes high-frequency components in a controlled, progressive manner, yielding latent codes that are smoother, more structured, and substantially easier to model. By training diffusion models on these spectrally denoised latents, we reduce optimization complexity and improve both stability and generation quality.

Specifically, we obtain a denoised latent representation  $z^{(\ell)} = \mathcal{S}_\ell(z)$  from the original  $z = \mathcal{E}(x)$  by suppressing its high-frequency components. The diffusion model is trained directly on this denoised latent rather than the raw, noise-contaminated one. Concretely, in the noise-prediction loss, we replace  $z$  with  $z^{(\ell)}$  at each training step. This process can be expressed as:

$$\min_{\theta} \mathbb{E}_{\ell, t, \epsilon} \left[ \left\| \epsilon_\theta(\sqrt{\bar{\alpha}_t} z^{(\ell)} + \sqrt{1 - \bar{\alpha}_t} \epsilon, t, c) - \epsilon \right\|_2^2 \right]. \quad (5)$$

where  $\epsilon_\theta(\cdot)$  is the network for predicting noise.  $\epsilon$  represents the actual noise.  $c$  denotes the conditional information.  $t$  represents the timestep of the denoising process.

### 3.3. Frequency-Domain Diffusion Alignment

Given a multi-level latent space, we accelerate training by letting a *cleaner, spectrally simpler* latent guide a *noisier, more complex* latent. Let  $z^{(\ell)} = \mathcal{S}_\ell(\mathcal{E}(x))$  be the level- $\ell$  attenuated latent, where larger  $\ell$  suppresses more high-frequency energy. At each iteration we sample  $(\ell_{\text{hi}}, \ell_{\text{lo}})$  with  $\ell_{\text{hi}} > \ell_{\text{lo}}$ , a diffusion timestep  $t$ , and noise  $\epsilon \sim \mathcal{N}(0, I)$ . The student sees a noisy, lower-attenuation latent,

$$\tilde{z}_t = \sqrt{\bar{\alpha}_t} z^{(\ell_{\text{lo}})} + \sqrt{1 - \bar{\alpha}_t} \epsilon, \quad (6)$$

while the teacher sees a clean, higher-attenuation latent  $\hat{z} = z^{(\ell_{\text{hi}})}$  at  $t=0$ . Intuitively, the teacher provides a spec-

trally simplified target that emphasizes global structure, giving the student a coarse-to-fine curriculum consistent with diffusion’s noise schedule. Let  $\epsilon_\theta(\cdot, t, c)$  be the diffusion network and  $\phi(\cdot, t, c)$  a selected intermediate feature. We follow SRA [19] to instantiate the teacher as an EMA of the student parameters, denoted  $\theta^-$ . The alignment loss matches student features to teacher features:

$$\mathcal{L}_{\text{align}} = \left\| \phi_\theta(\tilde{z}_t, t, c) - \phi_{\theta^-}(\hat{z}, 0, c) \right\|_2^2, \quad (7)$$

where the teacher branch is stop-gradient by construction. We add this alignment to the standard diffusion objective:

$$\mathcal{L} = \mathcal{L}_{\text{diff}} + \lambda_{\text{align}} \mathcal{L}_{\text{align}}. \quad (8)$$

We place higher weight on early timesteps via  $\lambda_{\text{align}}(t)$  to respect the coarse-to-fine schedule. The design accelerate the optimization of Denoising-VAE-based diffusion models.

## 4. Experiment

**Training.** All experiments are conducted on the ImageNet dataset [39], which contains 1.28M training images and 50K validation images. In the reconstruction stage, the tokenizer adopts a ViT-based encoder-decoder architecture and is trained with a batch size of 512 and a learning rate of  $1 \times 10^{-4}$ . We evaluate three configurations:  $f16d16$ ,  $f16d32$ , and  $f16d64$ , where  $f$  denotes the spatial downsampling factor and  $d$  denotes the number of latent channels. Under these settings, the Denoising-VAE is trained for 500K steps. In the generation stage, we use SiT-XL [31] as the diffusion model with the same tokenizer configurations. To reduce memory usage and improve training throughput, we precompute latent representations using the frozen Denoising-VAE and train SiT-XL directly on these latents without data augmentation. SiT-XL is trained with a batch size of 256 and a learning rate of  $1 \times 10^{-4}$ . SiT-XL is trained for 800 epochs in the main experiments and 80 epochs in ablation studies. Unless otherwise noted, all other hyperparameters are held constant across settings for fair comparison.

**Evaluation.** All evaluations are performed on the ImageNet validation split. For reconstruction, we report PSNR [18], SSIM [47], and LPIPS [57] as sample-level metrics, and FID [17] and sFID computed between reconstructions and the corresponding ground-truth images as distribution-level metrics. For image generation, we report FID and IS [40] under a unified evaluation protocol across all model variants and training strategies.

### 4.1. Denoising Facilitates a Balance Between Reconstruction and Generation

We conduct a comprehensive evaluation across three tokenizer configurations and nine training strategies to analyze reconstruction versus generation performance. As shown

Table 1. Reconstruction and generation performance. Notably, Denoising-VAE significantly improves generation quality while preserving reconstruction fidelity, with both 16- and 32-channel settings outperforming the original SD-VAE baseline. <sup>†</sup> Indicates using their VAE checkpoints, while the SiT training setting is kept identical to ours for a fair comparison. <sup>‡</sup> Indicates results reported in the original paper.

Tokenizer	Speed GFLOPs↓	Reconstruction Performance				Generation Performance			
		rFID↓	PSNR↑	IS↑	SSIM↑	gFID↓	sFID↓	IS↑	Pre.↑
<b>Conv-based tokenizer - f8d4</b>									
SD-VAE <sup>†</sup> [38]	445	0.62	26.04	–	0.834	18.01	5.13	74.29	0.64
EQ-VAE <sup>‡</sup> [26]	445	0.82	25.95	–	0.720	16.10	–	–	–
<b>ViT-based tokenizer - f16d16</b>									
MLSR	87.61	0.62	25.11	217.39	0.737	16.98	5.12	74.20	0.66
MLSR + Denoising	87.61	0.63	25.12	217.02	0.736	14.00	4.96	84.14	0.68
MLSR + Denoising + FDA	87.61	0.63	25.12	217.02	0.736	11.58	4.74	93.18	0.70
<b>ViT-based tokenizer - f16d32</b>									
MLSR	87.63	0.28	27.29	233.42	0.815	19.26	5.48	68.43	0.63
MLSR + Denoising	87.63	0.28	27.26	233.47	0.814	17.65	5.35	73.26	0.64
MLSR + Denoising + FDA	87.63	0.28	27.26	233.47	0.814	14.34	5.09	83.28	0.67
<b>ViT-based tokenizer - f16d64</b>									
MLSR	87.66	0.19	29.45	239.26	0.878	24.22	6.22	57.07	0.60
MLSR + Denoising	87.66	0.19	29.40	239.28	0.878	23.72	6.16	58.63	0.60
MLSR + Denoising + FDA	87.66	0.19	29.40	239.28	0.878	20.87	5.83	64.09	0.62

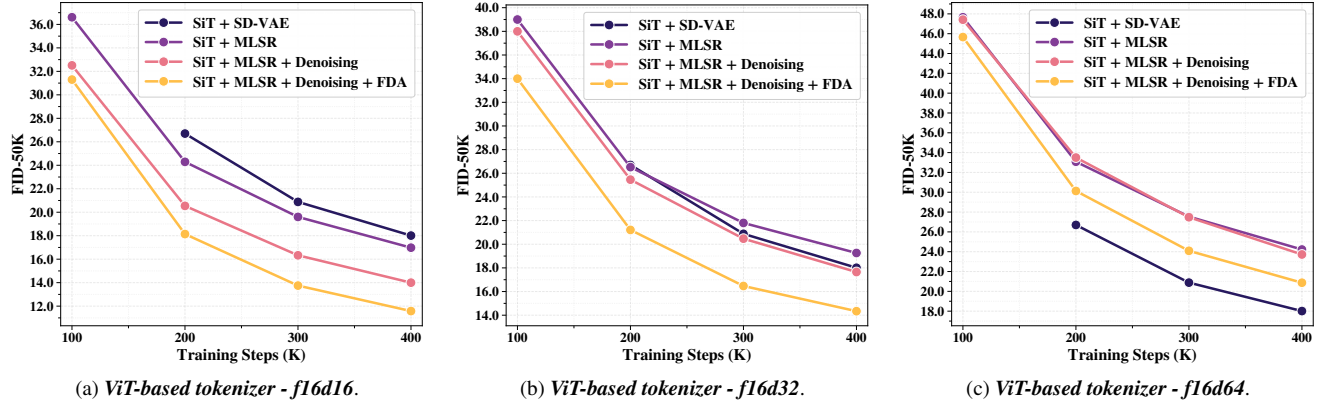


Figure 3. FID comparisons with vanilla SiT across different VAE settings on ImageNet 256 × 256 without CFG. Introducing denoising and frequency-domain alignment consistently improves convergence speed and generation quality across all latent dimensionalities.

in Table 1, increasing latent dimensionality consistently reduces rFID but raises gFID, indicating a tradeoff where stronger tokenizers improve reconstruction at the expense of generation quality. This observation substantiates the proposed optimization dilemma. Unless otherwise specified, "MLSR" refers to experiments conducted on improved latent representations  $\mathcal{E}(x)$  obtained via spectral regularization (see Section 3.1). "MLSR + Denoising" denotes the use of spectrally attenuated latents  $\tau \circ \mathcal{E}(x)$  to further suppress high-frequency noise (Section 3.2), while "MLSR + Denoising + FDA" combines these denoised latents with Frequency-Domain Alignment to guide the diffusion process (Section 3.3). Unless otherwise specified for ablation studies, we use the denoising level  $\ell = 2$  latent described in

Section 3.1 for all experiments.

**Denoising Preserves Reconstruction Fidelity.** Across all latent dimensionalities, our denoised latent representations achieve reconstruction metrics nearly identical to those of the baseline tokenizers, with PSNR differences below 0.05 dB and rFID differences under 0.01. This indicates that denoising primarily removes high-frequency components that have negligible impact on perceptual quality. As shown in Figure 2, PCA projections of the denoised latent space exhibit smoother spatial distributions and reduced high-frequency artifacts while preserving the structural information required for accurate decoding. Notably, even though the denoised latent is trained with a relaxed, perceptually equivalent reconstruction target, it still achieves high

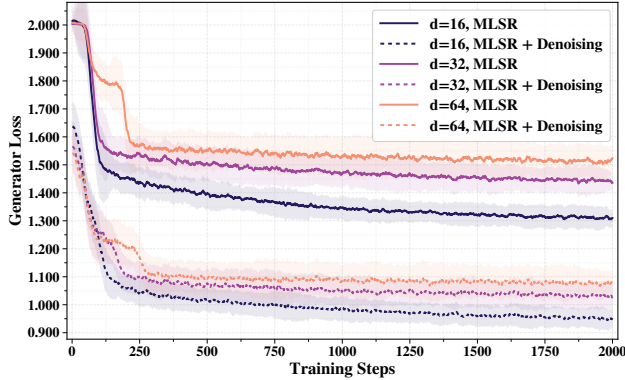


Figure 4. Training losses of tokenizers under different settings.

Table 2. Reconstruction performance on ImageNet 256 × 256. Metrics are computed from autoencoder outputs.

Tokenizer	Tokens	rFID $\downarrow$	PSNR $\uparrow$	SSIM $\uparrow$	LPIPS $\downarrow$
<b>Conv-based Tokenizer/Autoencoder</b>					
DC-AE [9]	64	0.77	23.93	0.766	0.092
VQVAE [45]	256	8.01	19.41	0.476	0.191
MaskGIT [5]	256	3.79	18.11	0.427	0.202
MaskBit [48]	256	1.29	21.07	0.539	0.142
VAVAE [53]	256	0.28	26.30	0.846	0.050
SD-VAE [38]	1024	0.62	26.04	0.834	–
SDXL-VAE [36]	1024	0.73	25.55	0.727	–
GaussToken [21]	1024	1.70	22.40	0.597	0.112
EQVAE [26]	1024	0.82	25.95	0.720	0.141
<b>ViT-based Tokenizer/Autoencoder</b>					
SoftVQ [8]	64	0.92	21.93	0.568	0.115
TiTok-B64 [54]	64	1.75	17.01	0.390	0.263
TiTok-S128 [54]	128	1.73	17.66	0.413	0.220
MAETok [7]	128	0.48	23.61	0.763	0.096
One-D-Piece [32]	256	1.54	17.74	0.420	0.210
FlexTok [1]	256	4.02	17.69	0.475	0.257
TexTok [56]	256	0.69	24.38	0.645	–
HieraTok [6]	256	0.45	–	–	–
Ours	256	<b>0.28</b>	<b>27.26</b>	0.815	0.091

fidelity. We hypothesize that this target’s reduced complexity leads to smaller prediction errors, whereas the original latent suffers larger errors due to its high-frequency noise.

**Denoising Accelerates and Stabilizes Optimization.** Beyond preserving reconstruction quality, latent denoising also brings benefits to downstream generative modeling. Across all configurations, models trained on denoised latents consistently achieve lower gFID scores under the same number of optimization steps. For example, our 32-channel VAE surpasses the original SD-VAE in generation performance. Moreover, as shown in Figure 3, denoised latents significantly accelerate training across tokenizer variants, reducing convergence time by up to 1.6 $\times$  compared to unregularized baselines. These improvements suggest that suppressing high-frequency noise produces a smoother and

more structured latent space, which facilitates diffusion optimization and enables faster, more stable learning. This confirms the effectiveness of spectral simplification as a regularization strategy in latent diffusion generation.

## 4.2. Alignment Improves Generation

As previously discussed, increasing tokenizer dimensionalities often leads to improved reconstruction but degraded generation, revealing a fundamental conflict in latent representation design. To address this challenge, we introduce Frequency-Domain Diffusion Alignment (FDA), which consistently improves convergence by guiding noisy latents using cleaner and spectrally simpler references. As shown in Table 1 and Figure 3, adding FDA consistently improves gFID across all tokenizer configurations and training durations, with gains remaining stable under equal training budgets. This improvement stems from a simple yet effective mechanism: spectrally simpler latents serve as guidance for their noisier counterparts, helping early denoising steps form meaningful structure more reliably. In effect, FDA introduces a progressive coarse-to-fine learning process in latent space, which accelerates convergence and improves final generative quality. In particular, FDA reduces convergence steps by up to 2 $\times$  compared to baselines.

## 4.3. Main Results

Under a unified experimental setting on the ImageNet 256 × 256 benchmark [39], we evaluate our Denoising-VAE against a diverse set of representative convolutional and ViT-based tokenizers. As evidenced by Table 2, Table 3 and Figure 5, our full method—combining Denoising-VAE with Frequency-Domain Diffusion Alignment—achieves an rFID of 0.28 and a PSNR of 27.26 for reconstruction, outperforming the strongest ViT-based alternative TexTok [56] by 2.88 dB in PSNR. At the same time, our method alleviates the optimization challenges inherent in high-dimensional latent spaces, substantially simplifying the training of diffusion models and significantly enhancing generative performance, achieving a competitive gFID of 1.82. Importantly, all improvements are achieved without any external semantic distillation. This indicates that supervision derived from spectrally denoised latents provides a more structured and learnable target, ultimately benefiting both optimization dynamics and final image quality.

## 4.4. Ablations and Discussions

### 4.4.1. Denoising Levels for Training Losses

As shown in Figure 4, we analyze training curves using different latent dimensionalities VAEs and observe two consistent trends. First, using lower-dimensional latents to train diffusion models leads to faster convergence and lower losses, indicating that diffusion becomes substantially easier to fit in simpler latent spaces. Second, at a fixed dimen-

Table 3. Comparison of reconstruction and generation performance on ImageNet at  $256 \times 256$  resolution. “Params” denotes the number of parameters in the generator (G) and tokenizer (T). Arrows indicate the direction of improvement for each metric.

Model	Params (G)	Params (T)	PSNR↑	rFID↓	gFID↓	IS↑	Pre.↑	Rec.↑
<b>With semantics distillation from external pretrained vision foundation models</b>								
<b>Conv-based tokenizer</b>								
SiT-XL + REPA [55]	675M	84M	26.04	0.62	1.42	305.7	0.80	0.64
LightningDiT + VA-VAE [53]	675M	84M	26.30	0.28	1.35	295.3	0.79	0.65
<b>ViT-based tokenizer</b>								
SiT-XL + MAETok [7]	675M	176M	23.61	0.48	1.67	311.2	–	–
LightningDiT + MAETok [7]	675M	176M	23.61	0.48	1.73	308.4	–	–
<b>Without semantics distillation from external pretrained vision foundation models</b>								
<b>Conv-based tokenizer</b>								
ADM-U [12]	731M	–	–	–	3.94	186.7	0.82	0.52
VDM++ [23]	2.0B	–	–	–	2.12	267.7	–	–
SoftVQ[8]	1.4B	72M	–	2.16	2.15	322.0	0.79	0.62
VAR-d30 [44]	2.0B	109M	–	0.90	1.92	323.1	0.82	0.59
LlamaGen-3B [43]	3.1B	72M	–	2.16	2.18	263.3	0.81	0.58
RandAR-XXL [34]	1.4B	72M	–	2.16	2.15	322.0	0.79	0.62
LDM-4 [38]	400M	55M	–	0.27	3.60	247.7	0.87	0.48
MaskDiT [58]	675M	84M	26.04	0.62	2.28	276.6	0.89	0.61
DiT-XL/2 [35]	675M	84M	26.04	0.62	2.27	278.2	0.83	0.57
SiT-XL/2 [31]	675M	84M	26.04	0.62	2.06	270.3	0.82	0.59
SiT-XL + DC-AE [9]	675M	323M	23.85	0.69	2.84	311.2	–	–
MAR-L + MAR-VAE [28]	479M	66M	–	1.22	1.78	296.0	0.81	0.60
MAR-H + MAR-VAE [28]	943M	66M	–	1.22	1.55	303.7	0.81	0.62
<b>ViT-based tokenizer</b>								
MAR-L + DeTok [51]	479M	171M	–	0.68	1.43	303.5	0.82	0.61
DiT-XL + HieraTok [6]	675M	176M	–	0.45	1.82	–	–	–
SiT-XL + Ours	675M	171M	<b>27.26</b>	<b>0.28</b>	1.82	274.1	0.81	0.61

sionality, using denoised latents to train diffusion models maintains lower losses than using raw latents. These observations show that, as dimensionality increases, accumulated high-frequency noise amplifies instability and slows convergence. They further demonstrate that suppressing redundant high-frequency components produces cleaner and better-conditioned latent representations, making them easier for diffusion models to optimize. Overall, the results highlight an inherent optimization dilemma in high-dimensional latent spaces and show that latent denoising effectively mitigates this issue while preserving both reconstruction fidelity and generative quality.

#### 4.4.2. Denoising Levels for Generation Performance

To systematically evaluate the effect of denoising strengths on generative performance, we conduct comparative experiments under a unified training and evaluation setup. Results in Table 4 show that under the *f16d16*, *f16d32*, and *f16d64* settings, a moderate denoising strength consistently reduces gFID, leading to smoother optimization while largely preserving reconstruction quality. When the denoising strength is further increased, gFID slightly rises in low- and mid-dimensional settings and even exceeds the no-denoising baseline in high-dimensional cases. We attribute this to

Table 4. Ablation study on different denoising levels. Moderate denoising balances reconstruction and generation.

Tokenizer	rFID↓	gFID↓	sFID↓	IS↑
<b>ViT-based tokenizer - f16d16</b>				
MLSR	0.62	16.98	5.12	74.19
MLSR + Denoising-level-1	0.62	13.76	4.75	82.41
MLSR + Denoising-level-2	0.63	14.00	4.96	84.14
MLSR + Denoising-level-3	1.07	14.62	5.71	80.46
<b>ViT-based tokenizer - f16d32</b>				
MLSR	0.28	19.26	5.48	68.43
MLSR + Denoising-level-1	0.28	17.55	5.30	72.76
MLSR + Denoising-level-2	0.28	17.65	5.35	73.26
MLSR + Denoising-level-3	0.67	17.98	5.52	71.51
<b>ViT-based tokenizer - f16d64</b>				
MLSR	0.18	24.22	6.22	57.07
MLSR + Denoising-level-1	0.18	23.86	6.22	57.16
MLSR + Denoising-level-2	0.19	23.72	6.16	58.63
MLSR + Denoising-level-3	0.55	25.67	6.48	53.35

the fact that excessive denoising, although making training easier and reducing loss values, shifts the latent feature distribution and weakens its structural consistency, thereby



Figure 5. Visualization Results. We visualize our latent diffusion system with proposed Denoising-VAE together with SiT-XL trained on ImageNet 256 × 256 resolution using classifier-free guidance with  $\omega = 1.8$ .

Table 5. Ablation study on alignment methods. Our FDA achieves better convergence and generation quality than other strategies.

Tokenizer	gFID↓	sFID↓	IS↑
<b><i>ViT-based tokenizer - f16d32</i></b>			
MLSR + Denoising	17.65	5.35	73.26
MLSR + Denoising + SRA [19]	15.44	5.12	78.90
MLSR + Denoising + FDA	14.34	5.09	83.28

degrading both reconstruction and generation. Overall, a moderate denoising strength effectively suppresses redundant noise in high-dimensional latent spaces while preserving essential structural and energetic components, achieving a better balance between stability and representational capacity in both reconstruction and generation.

#### 4.4.3. Alignment for Generation Performance

To verify the effectiveness of our proposed spectral alignment strategy, we compare it with standard self-alignment methods. Specifically, following SRA [19], we use two latents with the same denoising frequency as mutual guidance during training. As shown in Table 5, our method consistently achieves lower gFID scores than both the baseline and the SRA-based alignment method, indicating superior generation performance. We attribute this improvement to the fact that diffusion models inherently follow a coarse-to-fine generation process. Directly aligning different representations of the same latent disrupts this progression.

#### 4.4.4. Denoising Beats Equivariance Regularization

To verify the advantage of the denoising approach over the equivariance-regularized method, we design and conduct a set of comparative experiments. As shown in Table 6, without applying FDA, our method significantly outperforms the

Table 6. Comparison between EQ-VAE and Ours under a low-dimensional latent space. Columns denote different training steps.

Method	100k steps		200k steps		400k steps	
	gFID↓	IS↑	gFID↓	IS↑	gFID↓	IS↑
<b><i>Low-dimensional tokenizer</i></b>						
EQ-VAE [26]	41.3	30.9	24.9	54.6	16.1	79.7
Denoising-VAE	32.5	37.8	20.5	60.8	14.0	84.1

equivariance-regularized baseline [26] in low-dimensional latent spaces. This result indicates that, compared to indirectly constraining the representations via equivariance regularization, directly suppressing high-frequency noise in the latent space is a more effective design strategy.

## 5. Conclusion

In this work, we introduce Denoising-VAE, a ViT-based and VFM-free autoencoder that regularizes high-dimensional latent spaces through Spectral Self-Regularization. Beyond the architectural efficiency gains over convolutional VAEs (reducing GFLOPs by  $5.75\times$ ), we systematically reveal that the reconstruction-generation trade-off originates from redundant high-frequency noise in high-dimensional latents. By suppressing these components, Denoising-VAE simplifies the latent space, preserves reconstruction fidelity, and substantially improves generative performance. We further propose a Spectral Alignment strategy that enables diffusion models trained on Denoising-VAE latents to converge nearly  $2\times$  faster than those using SD-VAE. Extensive experiments validate the effectiveness of our framework. In future work, we plan to further investigate the intrinsic structure of high-dimensional latent spaces and develop more advanced spectral regularization techniques to

better unify reconstruction and generation performance.

## References

[1] Roman Bachmann, Jesse Allardice, David Mizrahi, Enrico Fini, Oguzhan Fatih Kar, Elmira Amirloo, Alaaeldin El-Nouby, Amir Zamir, and Afshin Dehghan. Flextok: Resampling images into 1d token sequences of flexible length. *CoRR*, 2025. 6

[2] Dor Bank, Noam Koenigstein, and Raja Giryes. Autoencoders. *CoRR*, 2020. 1

[3] Johann Brehmer, Sönke Behrends, Pim de Haan, and Taco Cohen. Does equivariance matter at scale? *TMLR*, 2025. 1

[4] Mathilde Caron, Hugo Touvron, Ishan Misra, Hervé Jégou, Julien Mairal, Piotr Bojanowski, and Armand Joulin. Emerging properties in self-supervised vision transformers. In *ICCV*, 2021. 1

[5] Huiwen Chang, Han Zhang, Lu Jiang, Ce Liu, and William T. Freeman. Maskgit: Masked generative image transformer. In *CVPR*, 2022. 1, 2, 6

[6] Cong Chen, Ziyuan Huang, Cheng Zou, Muzhi Zhu, Kaixiang Ji, Jiajia Liu, Jingdong Chen, Hao Chen, and Chunhua Shen. Hieratok: Multi-scale visual tokenizer improves image reconstruction and generation. *CoRR*, 2025. 6, 7

[7] Hao Chen, Yujin Han, Fangyi Chen, Xiang Li, Yidong Wang, Jindong Wang, Ze Wang, Zicheng Liu, Difan Zou, and Bhiksha Raj. Masked autoencoders are effective tokenizers for diffusion models. *CoRR*, 2025. 1, 2, 6, 7

[8] Hao Chen, Ze Wang, Xiang Li, Ximeng Sun, Fangyi Chen, Jiang Liu, Jindong Wang, Bhiksha Raj, Zicheng Liu, and Emad Barsoum. Softvq-vae: Efficient 1-dimensional continuous tokenizer. In *CVPR*, 2025. 2, 6, 7

[9] Junyu Chen, Han Cai, Junsong Chen, Enze Xie, Shang Yang, Haotian Tang, Muyang Li, and Song Han. Deep compression autoencoder for efficient high-resolution diffusion models. In *ICLR*, 2025. 2, 6, 7

[10] Junyu Chen, Dongyun Zou, Wenkun He, Junsong Chen, Enze Xie, Song Han, and Han Cai. DC-AE 1.5: Accelerating diffusion model convergence with structured latent space. *CoRR*, 2025. 1, 2

[11] Yinbo Chen, Rohit Girdhar, Xiaolong Wang, Sai Saketh Rambhatla, and Ishan Misra. Diffusion autoencoders are scalable image tokenizers. *CoRR*, 2025. 1

[12] Prafulla Dhariwal and Alexander Quinn Nichol. Diffusion models beat gans on image synthesis. In *NeurIPS*, 2021. 7

[13] Alexey Dosovitskiy, Lucas Beyer, Alexander Kolesnikov, Dirk Weissenborn, Xiaohua Zhai, Thomas Unterthiner, Mostafa Dehghani, Matthias Minderer, Georg Heigold, Sylvain Gelly, Jakob Uszkoreit, and Neil Houlsby. An image is worth 16x16 words: Transformers for image recognition at scale. In *ICLR*, 2021. 1

[14] Patrick Esser, Robin Rombach, and Björn Ommer. Tampering transformers for high-resolution image synthesis. *CVPR*, 2021. 2, 3

[15] Patrick Esser, Sumith Kulal, Andreas Blattmann, Rahim Entezari, Jonas Müller, Harry Saini, Yam Levi, Dominik Lorenz, Axel Sauer, Frederic Boesel, Dustin Podell, Tim Dockhorn, Zion English, and Robin Rombach. Scaling rectified flow transformers for high-resolution image synthesis. In *ICML*, 2024. 1

[16] Kaiming He, Xinlei Chen, Saining Xie, Yanghao Li, Piotr Dollár, and Ross B. Girshick. Masked autoencoders are scalable vision learners. In *CVPR*, 2022. 1

[17] Martin Heusel, Hubert Ramsauer, Thomas Unterthiner, Bernhard Nessler, and Sepp Hochreiter. Gans trained by a two time-scale update rule converge to a local nash equilibrium. In *NeurIPS*, 2017. 4

[18] Alain Horé and Djemel Ziou. Image quality metrics: PSNR vs. SSIM. In *ICPR*, 2010. 4

[19] Dengyang Jiang, Mengmeng Wang, Liuzhuozheng Li, Lei Zhang, Haoyu Wang, Wei Wei, Guang Dai, Yanning Zhang, and Jingdong Wang. No other representation component is needed: Diffusion transformers can provide representation guidance by themselves. *CoRR*, 2025. 4, 8

[20] Justin Johnson, Alexandre Alahi, and Li Fei-Fei. Perceptual losses for real-time style transfer and super-resolution. In *ECCV*. 3

[21] Bernhard Kerbl, Georgios Kopanas, Thomas Leimkühler, and George Drettakis. 3d gaussian splatting for real-time radiance field rendering. *TOG*, 2023. 6

[22] Maciej Kilian, Varun Jampani, and Luke Zettlemoyer. Computational tradeoffs in image synthesis: Diffusion, masked-token, and next-token prediction. *CoRR*, 2024. 1

[23] Diederik P. Kingma and Ruiqi Gao. Understanding diffusion objectives as the ELBO with simple data augmentation. In *NeurIPS*, 2023. 7

[24] Diederik P. Kingma and Max Welling. Auto-encoding variational bayes. In *ICLR*, 2014. 1, 2

[25] Diederik P. Kingma and Max Welling. An introduction to variational autoencoders. *Foundations and Trends in Machine Learning*, 2019. 2

[26] Theodoros Kouzelis, Ioannis Kakogeorgiou, Spyros Gidaris, and Nikos Komodakis. EQ-VAE: equivariance regularized latent space for improved generative image modeling. *CoRR*, 2025. 3, 5, 6, 8

[27] Hyomin Lee, Minseon Kim, Sangwon Jang, Jongheon Jeong, and Sung Ju Hwang. Enhancing variational autoencoders with smooth robust latent encoding. *CoRR*, 2025. 2

[28] Tianhong Li, Yonglong Tian, He Li, Mingyang Deng, and Kaiming He. Autoregressive image generation without vector quantization. In *NeurIPS*, 2024. 7

[29] Xiang Li, Kai Qiu, Hao Chen, Jason Kuen, Jiuxiang Gu, Bhiksha Raj, and Zhe Lin. Imagefolder: Autoregressive image generation with folded tokens. In *ICLR*, 2025. 1

[30] Zhuang Liu, Hanzi Mao, Chao-Yuan Wu, Christoph Feichtenhofer, Trevor Darrell, and Saining Xie. A convnet for the 2020s. In *CVPR*, 2022. 3

[31] Nanye Ma, Mark Goldstein, Michael S. Albergo, Nicholas M. Boffi, Eric Vanden-Eijnden, and Saining Xie. Sit: Exploring flow and diffusion-based generative models with scalable interpolant transformers. In *ECCV*, 2024. 1, 2, 4, 7

[32] Keita Miwa, Kento Sasaki, Hidehisa Arai, Tsubasa Takahashi, and Yu Yamaguchi. One-d-piece: Image tokenizer meets quality-controllable compression. *CoRR*, 2025. 6

[33] Maxime Oquab, Timothée Darct, Théo Moutakanni, Huy V. Vo, Marc Szafraniec, Vasil Khalidov, Pierre Fernandez, Daniel Haziza, Francisco Massa, Alaaeldin El-Nouby, Mido Assran, Nicolas Ballas, Wojciech Galuba, Russell Howes, Po-Yao Huang, Shang-Wen Li, Ishan Misra, Michael Rabbat, Vasu Sharma, Gabriel Synnaeve, Hu Xu, Hervé Jégou, Julien Mairal, Patrick Labatut, Armand Joulin, and Piotr Bojanowski. Dinov2: Learning robust visual features without supervision. *TMLR*, 2024, 2024. 1

[34] Ziqi Pang, Tianyuan Zhang, Fujun Luan, Yunze Man, Hao Tan, Kai Zhang, William T. Freeman, and Yu-Xiong Wang. Randar: Decoder-only autoregressive visual generation in random orders. In *CVPR*, 2025. 7

[35] William Peebles and Saining Xie. Scalable diffusion models with transformers. In *ICCV*, 2023. 1, 2, 7

[36] Dustin Podell, Zion English, Kyle Lacey, Andreas Blattmann, Tim Dockhorn, Jonas Müller, Joe Penna, and Robin Rombach. SDXL: improving latent diffusion models for high-resolution image synthesis. In *ICLR*, 2024. 1, 2, 6

[37] Alec Radford, Jong Wook Kim, Chris Hallacy, Aditya Ramesh, Gabriel Goh, Sandhini Agarwal, Girish Sastry, Amanda Askell, Pamela Mishkin, Jack Clark, Gretchen Krueger, and Ilya Sutskever. Learning transferable visual models from natural language supervision. In *ICML*, 2021. 1

[38] Robin Rombach, Andreas Blattmann, Dominik Lorenz, Patrick Esser, and Björn Ommer. High-resolution image synthesis with latent diffusion models. In *CVPR*, 2022. 1, 2, 5, 6, 7

[39] Olga Russakovsky, Jia Deng, Hao Su, Jonathan Krause, Sanjeev Satheesh, Sean Ma, Zhiheng Huang, Andrej Karpathy, Aditya Khosla, Michael S. Bernstein, Alexander C. Berg, and Li Fei-Fei. Imagenet large scale visual recognition challenge. *IJCV*, 2015. 4, 6

[40] Tim Salimans, Ian J. Goodfellow, Wojciech Zaremba, Vicki Cheung, Alec Radford, and Xi Chen. Improved techniques for training gans. In *NeurIPS*, 2016. 4

[41] Karen Simonyan and Andrew Zisserman. Very deep convolutional networks for large-scale image recognition. In *ICLR*, 2015. 3

[42] Ivan Skorokhodov, Sharath Girish, Benran Hu, Willi Menapace, Yanyu Li, Rameen Abdal, Sergey Tulyakov, and Aliaksandr Siarohin. Improving the diffusability of autoencoders. *CoRR*, 2025. 3

[43] Peize Sun, Yi Jiang, Shoufa Chen, Shilong Zhang, Bingyue Peng, Ping Luo, and Zehuan Yuan. Autoregressive model beats diffusion: Llama for scalable image generation. *CoRR*, 2024. 7

[44] Keyu Tian, Yi Jiang, Zehuan Yuan, Bingyue Peng, and Liwei Wang. Visual autoregressive modeling: Scalable image generation via next-scale prediction. In *NeurIPS*, 2024. 7

[45] Aäron van den Oord, Oriol Vinyals, and Koray Kavukcuoglu. Neural discrete representation learning. In *NeurIPS*, 2017. 2, 6

[46] Ashish Vaswani, Noam Shazeer, Niki Parmar, Jakob Uszkoreit, Llion Jones, Aidan N. Gomez, Łukasz Kaiser, and Illia Polosukhin. Attention is all you need. In *NeurIPS*, 2017. 1

[47] Zhou Wang, Alan C. Bovik, Hamid R. Sheikh, and Eero P. Simoncelli. Image quality assessment: from error visibility to structural similarity. *TIP*, 2004. 4

[48] Mark Weber, Lijun Yu, Qihang Yu, Xueqing Deng, Xiaohui Shen, Daniel Cremers, and Liang-Chieh Chen. Maskbit: Embedding-free image generation via bit tokens. *TMLR*, 2024. 6

[49] Pingyu Wu, Kai Zhu, Yu Liu, Longxiang Tang, Jian Yang, Yansong Peng, Wei Zhai, Yang Cao, and Zheng-Jun Zha. Alitok: Towards sequence modeling alignment between tokenizer and autoregressive model. *CoRR*, 2025. 2

[50] Tianwei Xiong, Jun Hao Liew, Zilong Huang, Jiashi Feng, and Xihui Liu. Gigatok: Scaling visual tokenizers to 3 billion parameters for autoregressive image generation. *CoRR*, 2025. 2

[51] Jiawei Yang, Tianhong Li, Lijie Fan, Yonglong Tian, and Yue Wang. Latent denoising makes good visual tokenizers. *CoRR*, 2025. 7

[52] Jingfeng Yao, Cheng Wang, Wenyu Liu, and Xinggang Wang. Fasterdit: Towards faster diffusion transformers training without architecture modification. In *NeurIPS*, 2024. 1

[53] Jingfeng Yao, Bin Yang, and Xinggang Wang. Reconstruction vs. generation: Taming optimization dilemma in latent diffusion models. In *CVPR*, 2025. 1, 2, 3, 6, 7

[54] Qihang Yu, Mark Weber, Xueqing Deng, Xiaohui Shen, Daniel Cremers, and Liang-Chieh Chen. An image is worth 32 tokens for reconstruction and generation. In *NeurIPS*, 2024. 6

[55] Sihyun Yu, Sangkyung Kwak, Huiwon Jang, Jongheon Jeong, Jonathan Huang, Jinwoo Shin, and Saining Xie. Representation alignment for generation: Training diffusion transformers is easier than you think. In *ICLR*, 2025. 7

[56] Kaiwen Zha, Lijun Yu, Alireza Fathi, David A. Ross, Cordelia Schmid, Dina Katabi, and Xiuye Gu. Language-guided image tokenization for generation. In *CVPR*, 2025. 2, 6

[57] Richard Zhang, Phillip Isola, Alexei A. Efros, Eli Shechtman, and Oliver Wang. The unreasonable effectiveness of deep features as a perceptual metric. In *CVPR*, 2018. 4

[58] Hongkai Zheng, Weili Nie, Arash Vahdat, and Anima Anandkumar. Fast training of diffusion models with masked transformers. *TMLR*, 2024. 7

[59] Jinghao Zhou, Chen Wei, Huiyu Wang, Wei Shen, Cihang Xie, Alan L. Yuille, and Tao Kong. ibot: Image BERT pre-training with online tokenizer. *CoRR*, 2021. 1